

Manuel Orlandi¹

Basic principles of substrate activation through non-covalent bond interactions

¹ Dipartimento di Scienze Chimiche, Università degli Studi di Padova, via Marzolo 1, Padova 35131, Italy, E-mail: manuel.orlandi@unipd.it. <https://orcid.org/0000-0002-0569-6719>.

Abstract:

In the last twenty years, chiral Brønsted acid and chiral counteranion catalysis have emerged as a fundamental area of organocatalysis. The development of chiral acidic catalysts has allowed extending many known Brønsted catalyzed reactions to the stereoselective domain. Moreover, the controlled conditions under which these catalysts can be used, allowed accessing reactivity of increasing complexity with extraordinary selectivity levels. However, compared to the explosion of this branch of organocatalysis in an applicative direction, only little has been done to understand and rationalize the observed reaction outcomes. This is due, in part, to the complex nature of the weak interactions (H-bonds, electrostatic, and dispersion interactions) governing this class of reactions. Here we review relevant mechanistic analyses from both chiral Brønsted acid and chiral counteranion directed catalysis. Both experimental and computational work is included that aimed at unveiling the nature of the interactions governing the a number of reactions. These include the: enantioselective reduction of ketoimines with Hantzsch esters; ring opening reactions of epoxides, oxetanes, aziridinium, and sulfonium ions; stereoselective fluorination of allylic alcohols; oxidative aminations of benzylic thioethers (enantioselective Pummerer reaction). These case studies are analyzed and discussed in order to highlight key features and similarities across the different catalytic systems.

Keywords: chiral Brønsted acid catalysis, chiral counteranion catalysis, mechanistic studies, H-bonding, non-covalent interactions

DOI: 10.1515/psr-2018-0090


1 Introduction

Brønsted acid catalysis has been known from a long time as a powerful tool for the promotion of chemical transformations. In particular, acidic compounds have been employed primarily as catalysts for the formation and cleavage of C-O and C-N bonds, as in hydrolysis and formation of esters, acetals, imines, and other simple functional groups. However, during the first years 2000, Brønsted acids, and especially Chiral Phosphoric Acids (CPAs), emerged as efficient catalysts for a range of more valuable transformations involving the formation of C-C bonds. Indeed, today Chiral Brønsted Acids (CBAs) are known to activate carbonyls, imines, alkenes, alkynes, and hydroxyl groups towards the attack of nucleophilic species in stereoselective fashion. Due to these important developments, an increasing attention has been devoted to the development of new CBAs, resulting in dozens of new catalysts able to promote hundreds of stereoselective transformations. However, compared to the explosion of this branch of organocatalysis in an applicative direction, only little has been done to understand and rationalize the observed reaction outcomes. This is due, in part, to the complex nature of the weak interactions (H-bonds, electrostatic and dispersion interactions) governing this class of reactions.

This chapter is a collection of the most relevant studies performed in the areas of CBA and chiral counteranion catalysis. All of the experimental work aimed at determining the catalysts acidity and at understanding the chemical activation of electrophilic substrates is included in Section 2.1. Section 2.2 collects NMR and electrochemical studies that revealed the nature of the H-bond coordination between CPAs and imines. It also contains a summary of the theoretical investigations of the stereoselective reduction of imines with Hantzsch esters from several authors. From Sections 2.3 through Sections 2.5 summarize the computational studies performed to rationalize the stereochemical outcome of other reactions including: ring opening reactions, pericyclic reactions and oxidations. Sections 3.1 through Sections 3.4 collect mechanistic studies of counter-anion directed catalysis that is reactions which do not involve Brønsted acidic activation of the substrate, but that proceed in stereoselective fashion due to tight pairing of the chiral anionic catalyst and a cationic reaction intermediate. The case studies included are (i) ring opening of *meso*-aziridinium and sulfonium ions, (ii) stereoselective fluorination of allylic alcohols, (iii) oxidative aminations of benzylic thioethers (enantioselective Pummerer reaction).

Manuel Orlandi is the corresponding author.

© 2020 Walter de Gruyter GmbH, Berlin/Boston.

Open Access. © 2018 The Author(s), published by De Gruyter. 

This work is licensed under the Creative Commons Attribution 4.0 International License.

2 Chiral Brønsted Acid (CBA) catalysis

2.1 H-bond activation and pK_a

The reaction rate of Brønsted acid catalyzed reactions have been shown long ago to correlate with the pK_a value of the reaction catalyst, in agreement with the Brønsted catalysis law (Figure 1) [1]. Importantly, the proportionality constant α provides useful information as its magnitude suggests the degree of proton transfer at the transition state (TS) level thus distinguishing between reactions proceeding via H-bond catalysis (H^+ still located on the catalyst anion A^- in the TS, Figure 1) or ion pairing (H^+ almost completely transferred to the substrate S in the TS, Figure 1). In both cases, activation of the substrate occurs via lowering of the substrate's Lowest Unoccupied Molecular Orbital (LUMO) energy, even though the effect is more pronounced in the case of complete proton transfer (ion pairing).

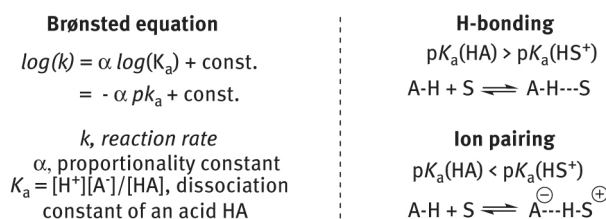


Figure 1: Brønsted equation, H-bonding and Ion pairing.

The degree of proton transfer does not only depend on the catalyst acidity, but also on the substrate basicity. As a rule of thumb, the pK_a of the catalyst has to be lower or at least of similar order of magnitude than the substrate's pK_a (acidity of the substrate's conjugated acid) in order to access a protonated (or activated) intermediate for catalysis (Figure 1). Knowing the pK_a values of Brønsted acid catalysts is therefore of high importance in order to establish *a priori* whether a certain acid will be suitable for substrate activation in a certain reaction.

The pK_a values of a wide range of acidic compounds in water are known. However, since most organic reactions are typically run in non-aqueous solvents, several groups established pK_a scales in media such as DMSO, MeCN or DCE. The most recent and comprehensive pK_a tables of strong Brønsted acids were collected by Leito and coworkers [2, 3]. The acidities of dozens of compounds within a pK_a range of 33 units (from 28 to -5) in MeCN were determined via spectroscopic titration methods [2]. Later, a similar *relative* scale of superacidic compounds was established in DCE [3].

In the context of stereoselective Brønsted acid catalysis, the pK_a values of a set of BINOL-based CBAs were first determined by O'Donoghue and Berkessel in 2011 by using UV-Vis methods and several indicators such as 4-nitrophenol, 2,4-dinitrophenol, 4-chloro-2,6-dinitrophenol and 2,4-dinitronaphthol in anhydrous DMSO [4]. The acidities of a similar set of compounds was determined in MeCN two years later by Leito and Rueping [5]. Some selected data from these two contributions are listed in Figure 2(a). These values suggest a clear acidity trend that mostly depends on the acidic functional group in compounds **1-3** and only marginally on the 3,3'-aryl substituents or on the BINOL scaffold (BINOL vs. $[H_8]$ -BINOL). In particular, bis-sulfonylimides **3** developed by Berkessel were found to be the most acidic compounds, followed by N-triflylphosphoramides **2** (NTPs) and by phosphoric acids **1**. This trend was also confirmed by the measurement of the reaction rates for the Nazarov cyclization catalyzed by several compounds chosen from the set, which were found to correlate with the catalysts' pK_a values in accordance with the Brønsted equation (Figure 2(b)) [5].

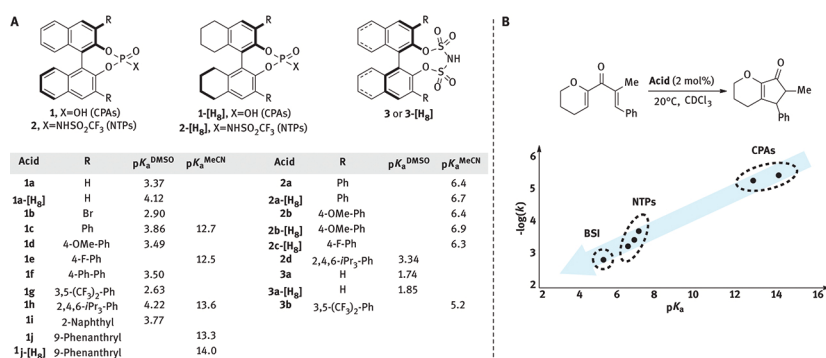


Figure 2: Common CBAs pK_a values, and correlation between catalyst's pK_a and reaction rate in a CBA-catalyzed Nazarov reaction.

Because of the rapid development of computational chemistry, the pK_a values of organic acids in solution can currently be calculated with similar accuracy than those determined experimentally [6, 7]. In 2013, a theoretical work appeared where Cheng and Li calculated the pK_a of a huge number of BINOL-derived phosphoric acids in DMSO [6]. The data reported by Berkessel were chosen as reference values, obtaining calculated pK_a values for additional 36 compounds. In particular, the pK_a values were found to range between 1.5 and 5.1 for CPAs, -3.1 and 1.9 for thiophosphoric acids (P(S)OH), and between -3.0 and -4.2 for dithiophosphoric acids (PS₂H). Despite in this first publication by Cheng and Li no information about NTPs or bis-sulfurylimides was provided, in a second paper published in 2014 by the same authors, new data completed the computational study [7]. Here the pK_a values of many additional acidic compounds were provided; in particular NTPs and bis-sulfurylimides were calculated to have pK_a of -3.9 to -2.2 and -3.7 to -2.3 , respectively. Hence, the calculations present a trend that is in agreement with the experimental data provided by Rueping and Leito in acetonitrile (i. e. pK_a bis-sulfurylimides $\leq pK_a$ NTPs $\ll pK_a$ CPAs) [5].

2.2 Stereoselective reduction of imines

Since the pioneer reports by Akiyama and Terada in 2004 [8, 9], which introduced the use of CPAs as organocatalysts, imines proved the most widely used substrates in CBA catalysis. This is likely due to the relatively high pK_a of this class of compounds, which allows for the addition of a huge range of nucleophiles. It is therefore not surprising that the very few experimental mechanistic studies performed in order to understand the chemical–physical basis of Brønsted acid catalysis involved phosphoric acids in combination with imines.

The very first work in this context is due to Gschwind and Rueping [10], who in 2011 reported the NMR characterization of the acid-base complex between phosphoric acid **4** and imines **5**. Elucidating the exact mechanisms involved in chiral phosphoric acid catalyzed systems is not an easy task due to the large number of possible interactions that could occur between the catalyst and the substrate. However, by performing an NMR characterization of the ¹⁵N-labeled adduct **6** (in toluene-*d*₈ as the solvent), the authors found three different species in solution: the H-bonded complex **6a**, the ion-pair complex **6b**, and the dissociated ion pair **6c** (Figure 3). Specifically, while at 300 K only one broad ¹H-NMR signal was detectable at ca. 16.2 ppm, by lowering the temperature this signal split in three broad signals. These signals became sharper as the temperature was further decreased to 240 K, at which temperature a singlet at $\delta = 18.16$ ppm and two doublets at $\delta = 15.50$ and 11.87 ppm with ¹J_{H,N} coupling constants of 86.01 and 69.5 Hz were observed. On the basis of further characterization (1D ³¹P, ¹H INEPT, 2D ¹H, ¹⁵N HMQC and ¹H DOSY), these signals were assigned respectively to **6a**, **6b** and **6c** (Figure 3).

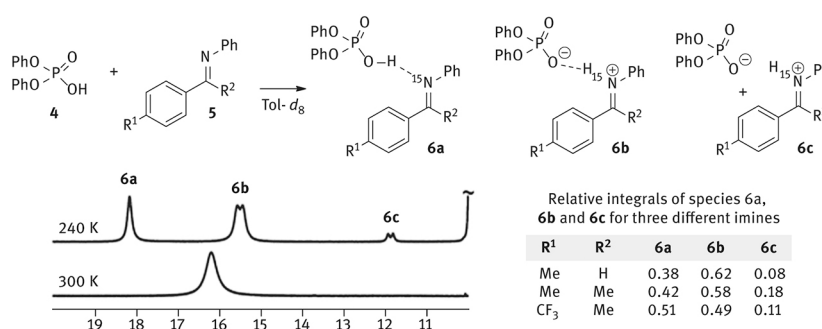


Figure 3: Speciation of CBA/imine complexes observed by ¹H NMR. Adapted with permission from *Angew. Chem. Int. Ed.* 2011, 50, 6364.

As expected, the authors found that reducing the nitrogen basicity of **5** by changing the imine's substituent R¹ and R², the **6a**:**6b** ratio slightly decreases. The tested substrates are reported in Figure 3 together with the **6a**:**6b**:**6c** relative amount of each species for each salt. From the table it can be observed how the ratio between the H-bond complex **6a** and the ion pair complex **6b** changes toward **6b** quite accordingly with the imines' basicity. On the other hand, the relative amount of **6c** with respect to **6a** and **6b** can be hardly rationalized.

Being able to evaluate the ability of a catalyst to protonate, coordinate or activate a substrate is of crucial importance. Since an iminium ion is more reactive than the relative imine, it can be pointed out that the greater is the **6a**:**6b** ratio, the more efficient is the activation of the substrate by the catalyst. At the same time, a tight ion pair is necessary to achieve higher stereoselectivities. Hence, the optimum conditions for the development of an efficient catalysis (both in terms of chemical and stereochemical activity) are related to the relative amount of the tight ion pair **6b** with respect to the H-bond complex **6a** and to the dissociated ion pair **6c**. In this context, Hunger and coworkers characterized and quantified the complex formation of **4** with 2-methylquinoline (of similar

basicity than imines) by combining dielectric spectroscopy, quantum chemistry, and ^1H NMR techniques [11]. For a series of different solvents, the interaction between substrate and catalyst was found to be dominated by ion-pairing, rather than hydrogen bonding.

Despite the useful insights gained by Gschwind and coworkers, the studies were complicated by peak broadening of the H-bond signals, which indicated broad conformational space and multiple aggregation states for the achiral catalyst **4**, which is poorly representative of the much bulkier structures of the most widely used catalysts (**1-2**). Thus, for a more detailed analysis, the more sterically hindered CPA **1h** (TRIP) was used [12]. Characterization of complexes **7** (Figure 4), revealed a slightly different scenario than previously observed with **6**. Specifically, the neutral H-bond and the dissociated ion pair complexes were not observed (with the only exception of one strongly electron-deficient imine). Additionally, two peaks for the hydrogen bonded ion pair **7** appeared upon temperature lowering in the ^1H , ^{15}N and ^{31}P spectra. These were assigned to the salts of the *Z*- and *E*- isomers of the imine (*E*-**7** and *Z*-**7**, Figure 4) based on NOESY experiments. This speciation was consistent through the set of imines used (10 examples) even though the *E*:*Z* ratio was found to be dependent on the nature of the imine aryl substituents.

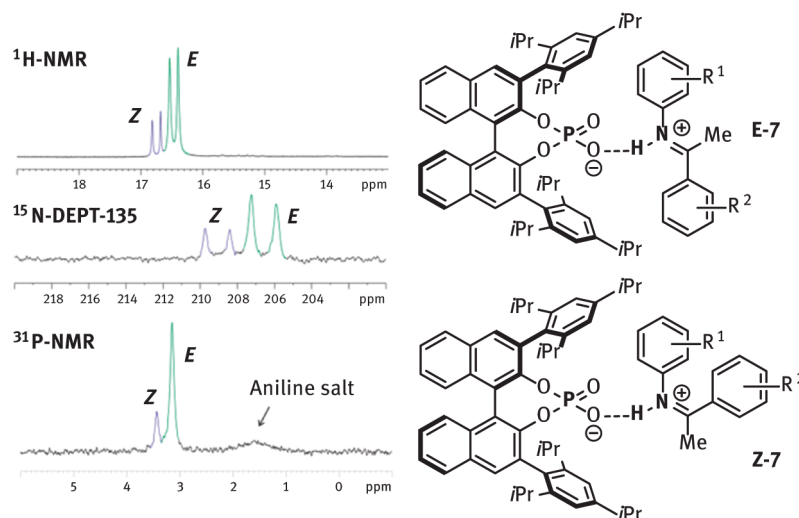


Figure 4: Speciation of TRIP/imine complexes observed by ^1H NMR. Adapted with permission from *J. Am. Chem. Soc.* **2016**, *138*, 16345.

Having established a methodology for accessing reliable NMR measurements for these complexes, the authors turned their attention to a more detailed study of the properties of the H-bond structure in solution. Based on the determination of ^1H and ^{15}N chemical shifts obtained from several combinations of 10 imines and 8 acids (phenols, carboxylic acids, **1h** and $\text{HBF}_4 \bullet \text{OEt}_2$), the authors were able to determine the geometry and the strength of the complexes' H-bonds using a methodology previously developed by Limbach and Denisov [13–16].

The formation of strong H-bonds is associated with a proton-transfer reaction between H-bond donor and acceptor. Hence, the faster the proton exchange between the two basic sites (O and N), the stronger the H-bond. In other words, the H-bond results to be weaker when the proton steadily resides on one of the two partners resulting into a more likely dissociation of the two basic partners (one of the two taking the proton). In ^1H NMR spectra, protons in *strong* or *low-barrier* H-bonds are usually observed for chemical shifts above 16 ppm. The plot in Figure 5 shows the Steiner-Limbach correlation of the ^1H chemical shift $\delta(\text{OHN})$ against the ^{15}N chemical shift $\delta(\text{OHN})$ of several complexes reported by Gschwind and coworkers. The parabolic dependence of the proton chemical shifts $\delta(\text{OHN})$ in combination with the linear dependence of the nitrogen chemical shifts $\delta(\text{OHN})$ allows the determination of the valence bond orders (p_{NH} and p_{OH}) by employing empirical correlations. From these, important geometric features can be derived, like the NH and OH bond length (r_{NH} and r_{OH}). The experimentally derived r_{NH} and r_{OH} were then compared with the computed NH and OH distances in the condensed phase (DCM), which were found to be in excellent agreement.

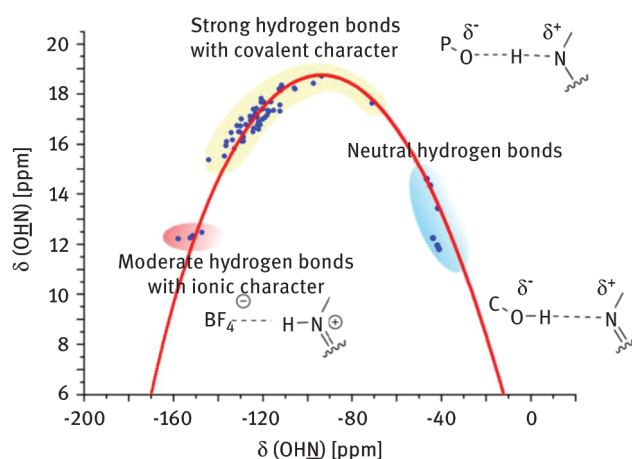


Figure 5: Steiner-Limbach correlation of the ^1H chemical shift $\delta(\text{OHN})$ against the ^{15}N chemical shift $\delta(\text{OHN})$ of several H-bond complexes. Adapted with permission from *Acc. Chem. Res.* **2017**, *50*, 2936.

Altogether, the collected data suggested the formation of a strong ionic H-bond between the catalyst **1h** and imine substrates **5**. This is explanatory of the good performance shown in terms of stereoselectivity when these catalysts and substrates are combined.

It is reasonable that the tight contact between **1h** and **5**, due to the presence of a strong H-bond, allows for other intermolecular interactions to take place. Gschwind and coworkers performed a conformational study of complexes *E-7* and *Z-7* separately using 1D ^1H , ^1H selective NOESY and ^1H , ^{19}F HOESY experiments and theoretical calculations [17]. Both complexes *E-7* and *Z-7* gave NOE patterns connecting both imine aryl groups and the catalyst binaphthyl backbone, while only for *Z-7* there were detectable contacts between the catalyst aryl substituents and the imine α -methyl group. The observed NOE patterns are highlighted with green (^{19}F , ^1H) or purple (^1H , ^1H) arrows in Figure 6, which shows the four conformations computed for the binary complexes *E-7* (two conformations, *Type I E* and *Type II E*) and *Z-7* (two conformations, *Type I Z* and *Type II Z*). Based on experiments and computations, the authors conclude that the energy barrier for the *Type I-Type II* transition is very low and allows free interconversion even at 180 K.

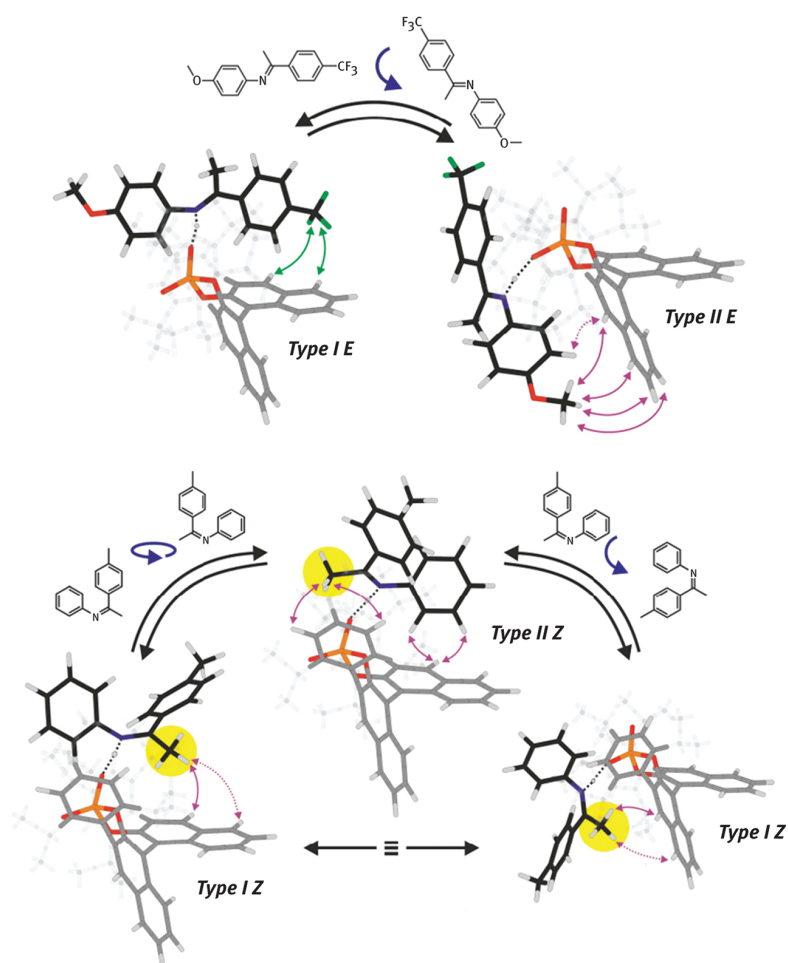


Figure 6: Computational/Spectroscopic (NMR) conformational analysis of two TRIP/imine complexes. Reproduced with permission from *J. Am. Chem. Soc.* **2016**, *138*, 15965.

Interestingly this study showed that molecular recognition in these binary complexes is due not only to a strong ionic H-bond between the acid and the imine, but also to non-covalent interactions (NCIs) such as CH- π and T-shaped π contacts between the imine aryl groups and the catalyst binaphthyl backbone. Sigman and Toste found a similar catalyst-substrate interaction occurring in the asymmetric fluorination of allylic alcohols as will be discussed in Section 3.4 of this chapter [18].

Information about the structure of pre-reacting binary complexes is extremely important for mechanistic insights. Nevertheless, the ultimate understanding of a stereo- or regioselective reaction outcome is given by the knowledge of the TSs, especially in Curtin–Hammett scenarios and kinetically controlled transformations. TSs can hardly be studied experimentally due to their evanescent nature. However, their structure can be computed and experimental insights about their properties can be obtained via kinetic probing of the reaction under exam. Gschwind et al. used their acquired knowledge in the field of CBA catalysis to study the reduction of imines catalyzed by CPAs with Hantzsch ester **8** previously reported by Rueping and List [19, 20].

This reaction was proposed to proceed through a ternary complex of the catalyst with the two reagents according with the cycle depicted in Figure 7(a). As previously described, the coordination of the imine to **1h** leads to complexes **E-7** and **Z-7**, both of which are eligible to react with the nucleophile **8** to give either the *R* (the observed major product) or the *S* product **9** according with one of the four possible pathways depicted in Figure 7(b) (**TS-E/R**, **TS-E/S**, **TS-Z/R**, **TS-Z/S**). To experimentally determine which one of these TSs is actually operating in catalysis, the authors developed a method that exploits light as an external stimulus (orthogonal to the reaction mechanism) to modulate the equilibrium of slowly interchanging complexes **E-7** and **Z-7** (Figure 7(c)). In other words, irradiation of the reaction mixture at a proper wavelength would induce isomerization of the imine from the *E* to the *Z* configuration thus altering the thermodynamic equilibrium of the reactants in favor of intermediate **Z-7**. If isomerization occurred at comparable or lower rate with respect to the reaction itself, the Curtin–Hammett boundaries would not be valid anymore. As a result, both the reaction outcomes (*ee* and reaction rate) could be affected by the change in the pre-reaction equilibrium in different ways depending on which reaction pathways are operating in catalysis. Thus, comparison of the reaction outcomes of the reaction performed in the dark and under light irradiation would reveal the operating TSs leading to each enantiomers of **9** according to the scheme in Figure 7(d). Since the reaction under light irradiation provided *identical ee's* but

higher reaction rates with respect to the control experiments in the dark, the authors concluded that the reaction proceeds via **TS-Z/R** and **TS-Z/S**, the former being the favorite one due to the observed absolute configuration of product **9**.

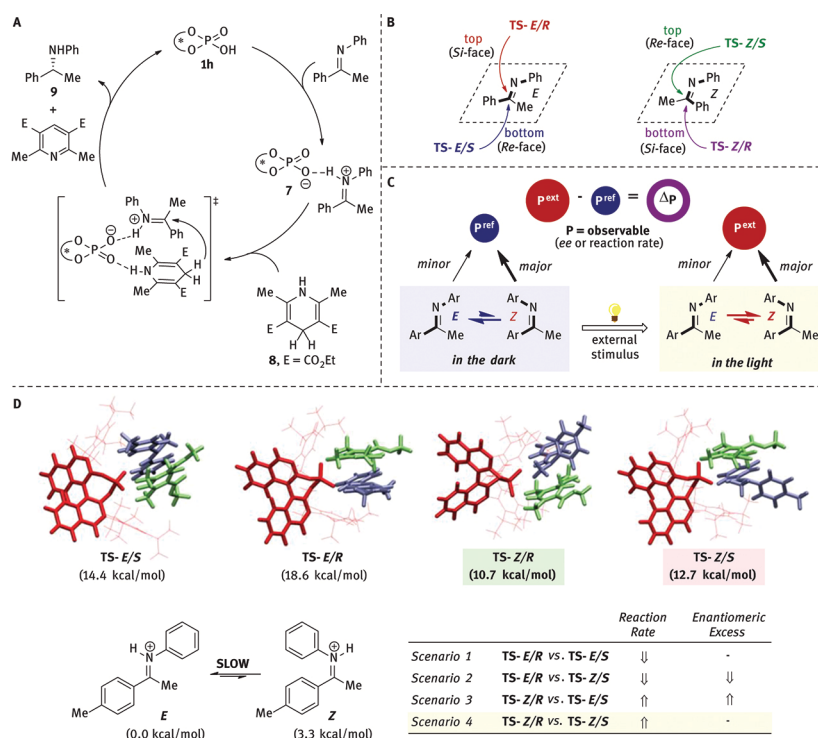


Figure 7: Experimental/computational study the reduction of imines catalyzed by CPAs with Hantzsch ester. Adapted with permission from *J. Am. Chem. Soc.* **2017**, 139, 6752.

In order to provide theoretical support to the observed experimental outcomes, **TS-E/R**, **TS-E/S**, **TS-Z/R** and **TS-Z/S** were computed. As the Curtin–Hammett principle was shown not to apply by the experiments (*vide infra*), the energy of the TSs should not be directly compared, but the activation barrier from the corresponding *E*- or *Z*-imine should be considered instead. The computed structures are reported in Figure 7(d) together with their corresponding Gibbs free energy barriers calculated from the corresponding imine energy level (0.0 vs. 3.3 kcal/mol for the *E* and *Z* imine respectively, Figure 7(d)). **TS-Z/R** and **TS-Z/S** were found to be the TSs with the lowest energy barrier leading to (*R*)-**9** and (*S*)-**9** (10.7 vs. 12.7 kcal/mol). The energy difference between the two TSs accounts for the experimental *ee* and, since both of them derive from the imine in the *Z* configuration, the computations also account for the increase in reaction rate observed under light irradiation.

These calculations by Gschwind and coworkers were found to be in line with previous contributions by Himo and Goodman [21–23]. However, the experimental work here reviewed allowed accessing experimental information about the actual operating TSs thus providing support to the computed reaction mechanism.

This mechanistic study from the Gschwind group was mainly focused on the use of catalyst **1h** (TRIP). Recent theoretical investigations of the role of the BINOL 3,3′ aryl substituents in the reduction of imines was recently provided by Goodman [24], whose team showed that the hydrogenation mechanism with Hantzsch esters is dependent on the proximal and distal steric hindrance of the catalyst substituents. In a correlated study of the CPA catalyzed Strecker reaction [25], Goodman showed that the configuration of the reacting imine is also dependent on the sterics of the substrate’s α -alkyl group. It was shown that while for ketimines the reaction typically proceeds with the substrate in the *Z* configuration, aldimines prefer to react in configuration *E*.

Altogether, the studies hereby reviewed show that the catalytic activity of CPAs is affected by a plethora of factors. These include:

- i. the catalyst’s acidity (low pK_a values ensure substrate activation);
- ii. the ability of the PO_2H group to effectively coordinate the imine N atom to form a strong H-bond;
- iii. the ability of the catalyst’s scaffold to engage the substrate in NCIs;
- iv. the size of the catalyst’s pocket (which can affect the substrate’s conformation in the binary complex).

As we will see through this chapter, the ability to control these factors proved to be crucial for developing efficient stereoselective transformations. Unfortunately, the coordination mode and the structure of the competing TSs is not easily accessible *a priori* for any reaction. Thus, establishing precedents and developing new physical-organic methodologies for gaining such information remains a task of great importance.

2.3 Ring opening reactions

2.3.1 Epoxides

A general rule of thumb states that Brønsted acid catalysis proceeds via coordination/activation of the reaction electrophile. The CPA-catalyzed epoxide and aziridine ring opening reactions (Figure 8(a)) developed by List and coworkers [26–30] are an exception to this rule. In these transformations, the catalyst coordinates the carboxylic acid **10**, the nucleophile, rather than the electrophilic epoxide **11** [26]. Specifically, the ^1H and ^{31}P NMR spectra of **1h** showed considerably shifted signals upon addition of a stoichiometric amount of benzoic or acetic acid. The translational diffusion coefficients of such mixtures were also found to be substantially different from those of the single components, thus suggesting complexation between the two partners. Additionally, the ^{31}P NMR titration experiments of **1h** with these acids resulted in the determination of the binding isotherm of association, which in turned allowed calculation of the binding constants ($K_a^{\text{BzOH}} = 3981 \pm 98 \text{ M}^{-1}$, $K_a^{\text{AcOH}} = 1948 \pm 26 \text{ M}^{-1}$, Figure 8(b)). Method of continuous variations and co-crystallization of AcOH and **1h** (X-ray analysis), revealed the formation of an equimolar complex (1:1 ratio) with structure **12**.

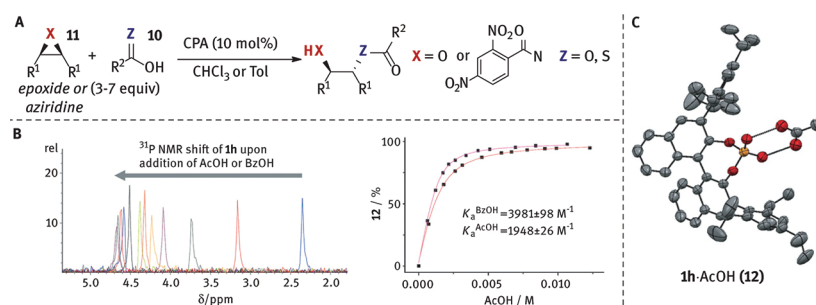


Figure 8: CPA-catalyzed epoxide and aziridine ring opening reaction. Adapted with permission from *Angew. Chem. Int. Ed.* 2014, 53, 7063.

Reactivity in CBA catalysis based on the electrophile activation is easily rationalized by invoking the lowering of the LUMO energy upon protonation by the catalyst. How do these reactions, proceeding via coordination of the nucleophile, work then? List and coworkers noticed that the ^{31}P chemical shift of **12** was shifted downfield with respect to **1h** alone, consistent with partial positive charge building up on the phosphate group. This is counterintuitive, as one would expect the more acidic compound (**1h**) to protonate the carboxylic acid and not *vice versa*. In other words, these NMR experiments seemed to suggest that the CPA behaves as a base within the complex, thus making the phosphate group more acidic and the carboxylic acid more nucleophilic in a synergistic activation. This was confirmed by computational evaluation of the HOMO and LUMO energies of free AcOH and of AcOH within complex **12**. While the LUMO energy change was calculated to be small ($\Delta E = +0.08 \text{ eV}$), the HOMO energy was significantly increased upon coordination ($\Delta E = +0.25 \text{ eV}$) [29].

The kinetic relevance of dimer **12** in catalysis was also established by determination of the epoxide opening reaction's rate law. The reaction rate was found to be first order in **13** and **1h**, but zeroth order in the carboxylic acid. This is consistent with the catalytic cycle depicted in Figure 9, where complex **12** is the catalyst resting state and reacts with epoxide **13** in the reaction rate- and stereo-determining step [29].

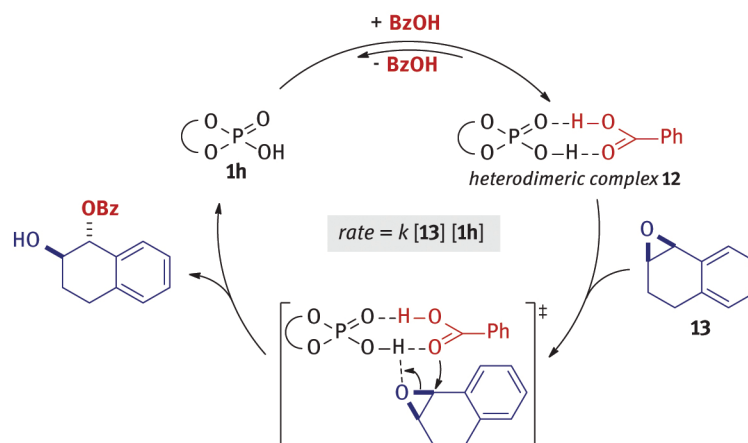


Figure 9: Mechanism of the CPA-catalyzed epoxide ring opening reaction.

The influence of the catalyst's structure on the enantioselectivity was investigated by DFT calculation of the reaction TSs for the opening reaction of the model system BzOH + **14** [29]. Catalysts **1h** and **1k** were considered for the calculations as they provided different catalytic activities in the opening reaction of cyclohexene oxide, (*S,S*)-**1k** being superior to (*S,S*)-**1h** (93 vs. 57% *ee*). The computed TSs showed the same general arrangement of the reagents within the catalyst chiral pocket. Specifically, the reagents complex are coordinated by the catalyst via two H-bonds and a strong electrostatic interaction between the electron-rich phosphoryl oxygen and the partially positively charged C-H moiety of the epoxide as previously found by Wheeler for a similar system [31]. Confined in the pocket by virtue of these attractive interactions, the electrophile also experiences steric repulsion from the isopropyl groups of (*S,S*)-**1h** and (*S,S*)-**1k**. The difference in selectivity between the two catalysts is due to a balance of these positive and negative contacts with the substrate. (*S,S*)-TS**1k-14** and (*S,S*)-TS**1h-14** in Figure 10 are the low lying energy TSs leading to both the (*R,R*)- and (*S,S*)-product for each catalyst. The computed $\Delta\Delta G^\ddagger$ was higher for catalyst **1k** (1.9 vs. 0.74 kcal/mol in the case of **1h**), thus reproducing the experimental relative performance of the two CPAs. A rationalization to the different $\Delta\Delta G^\ddagger$ was given based on the distance between the epoxide methyl substituent and the catalyst 3,3' groups, which was shorter in (*R,R*)-TS**1k-14** (4.56 Å) than in (*R,R*)-TS**1h-14** (4.78 Å). Specifically, the shortest distance (i. e. the strongest repulsive interaction) was observed in (*R,R*)-TS**1k-14** between the epoxide and the catalyst's polycyclic substituent in the *meta* position of the 3,3 aryl groups, which distinguish the structure of **1k** from **1h**.

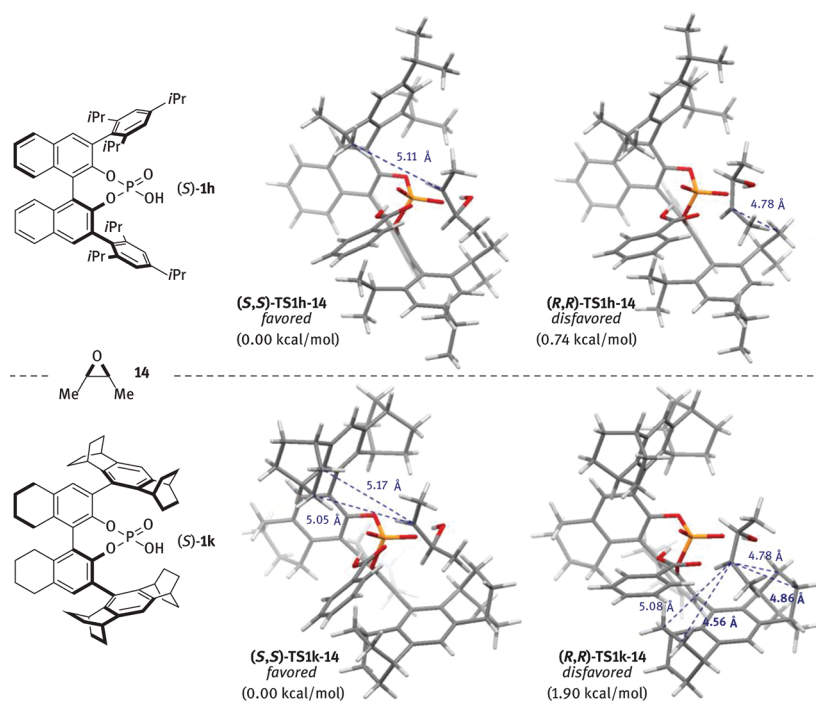


Figure 10: Computed TSs of the ring opening reaction of **14** catalyzed by **1h** and **1k**. Adapted with permission from *J. Am. Chem. Soc.* **2016**, *138*, 14740.

This study by List and coworkers showed that CPAs strongly coordinate carboxylic acids via H-bonding. This coordination leads to: (i) rising of the carboxylic HOMO energy, thus making it more nucleophilic and, consequently, to (ii) building up of positive charge on the phosphate moiety, thus making the catalyst more acidic. The binary complex thus formed is able to react with electrophiles like epoxides and aziridines to give diols and aminoalcohols, respectively. The reaction enantioselectivity was shown to be highly dependent on the steric environment provided by the catalyst's 3,3' groups. This was rationalized based on the balance of a *plethora* of attractive and repulsive NCIs that interplay at the TS level, sharing many general similarities with the case studies presented in the previous section.

2.3.2 Oxetanes

Oxetanes are strained four-membered rings that readily open in the presence of suited nucleophiles under CBA catalysis conditions as shown by Sun and coworkers (Figure 11) [32–34]. The intramolecular version of this transformation was developed first, which employs the SPINOL based CBA **15a** as the optimal catalyst (Figure 11(a)).

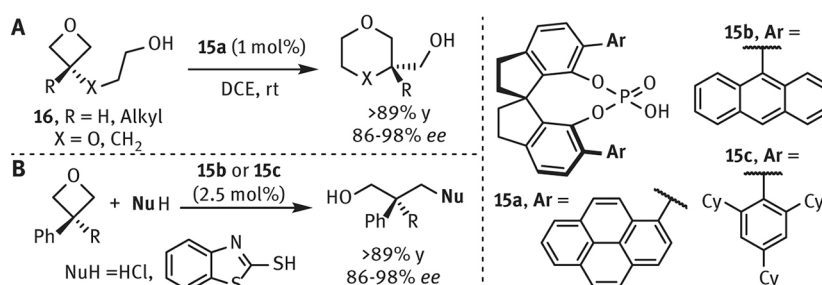


Figure 11: CPA-catalyzed oxetanes ring opening reaction.

The stereochemical outcome of this reaction was rationalized via DFT TS analysis by the groups of Wheeler and Houk [35], who showed that oxetanes **16** display a different mode of activation with respect to other common electrophiles in the presence of CPA **15a**. Specifically, it was found that in the favored TS leading to the major enantiomer (*S*)-**TS-16** the catalyst's acidic OH group coordinates/activates the oxetane O atom, the catalyst's basic site P=O is involved in an interaction with the four-membered ring H atoms. Thus, the catalyst is involved in the electrophilic activation of the substrate, while the nucleophilic OH group is only involved with an OH $\cdots\pi$ interaction with the catalyst's pyrenyl groups (Figure 12(a)). On the other hand, in the TS leading to the disfavored product (*R*)-**TS-16**, such a stabilizing interaction was weaker (2.58 vs 2.48 Å), and showed steric clashes between the ring substituents and the catalyst's 3,3'-aryl groups (Figure 12(b)). These structural differences between the diastereomeric TSs account for the computed $\Delta\Delta G^\ddagger \approx 2$ kcal/mol, in good agreement with the experimental selectivity.

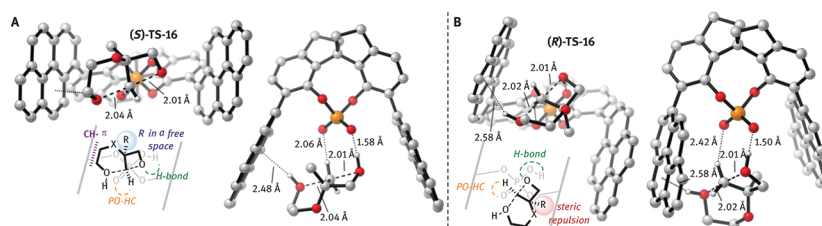


Figure 12: Computed TSs of the ring opening reaction of oxetane **16** catalyzed by CPA **15a**. Adapted with permission from *ACS Catal.* **2017**, *7*, 7332.

In 2016, Wheeler and Houk separately performed the computational study of the two intermolecular versions of the CPA catalyzed oxetane ring opening reaction in Figure 11(b) [31, 35]. The two studies show that, independently from the nucleophile, the oxetane ring coordination mode is preserved also in the case of intermolecular reactivity. However, differently from the intramolecular reaction, the attack of the external nucleophile is assisted by coordination of the P=O basic site (Figure 13(a)). Computation of the TSs leading to both the enantiomeric products for several substrates showed that a general stereochemical model is in place. Specifically, the catalyst's P=O group binds via PO-HC interaction to the oxetane methylene group that undergoes the addition. However, in the chiral environment provided by the catalyst, one of the two enantiotopic groups is coordinated preferentially due to the steric clash between the oxetane ring substituent R and the catalyst aryl group leading to the observed enantioselectivity (Figure 13(b)).

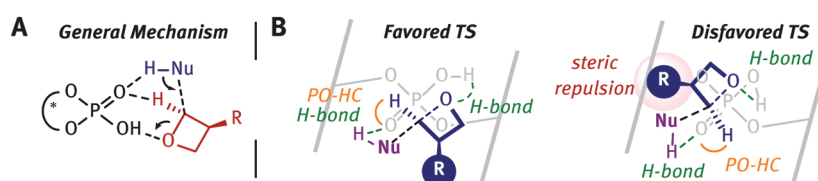


Figure 13: General stereochemical model for the CPA-catalyzed oxetanes ring opening reaction.

2.4 Asymmetric pericyclic reactions

2.4.1 [3±2]-cycloaddition of hydrazones

The [3+2]-cycloaddition between hydrazones and alkenes reported by Rueping and Houk is an example of N-triflylphosphoramidate (NTP) catalyzed reaction (Figure 14(a)) [37]. NTPs are more acidic (see Section 2.1) and able to activate a wider range of substrates than CPAs. The triflyl group (CF_3SO_2) offers a greater number of possible coordination sites and orientations than the simple OH group. Additionally, the presence of two different substituents at the P atom reduces the symmetry of the catalyst from C₂ (for CPAs) to C₁. Consequently, the number of possible conformers and coordination modes increases considerably, making the computational study of reactions catalyzed by NTP more difficult. Therefore, Houk and coworkers began their study with a conformational analysis of the complex **19** formed between the model NTP **17** and hydrazone **18** (Figure 14(b)). Among all of the possible conformers, **19a–19d** were found to have the lowest energies. Therefore, these coordination modes were investigated as possible reaction partners of ethyl vinyl sulfide. **19c** was calculated to be the most reactive conformer toward ethylene, with a $\Delta G^\ddagger = 28.6$ kcal/mol.

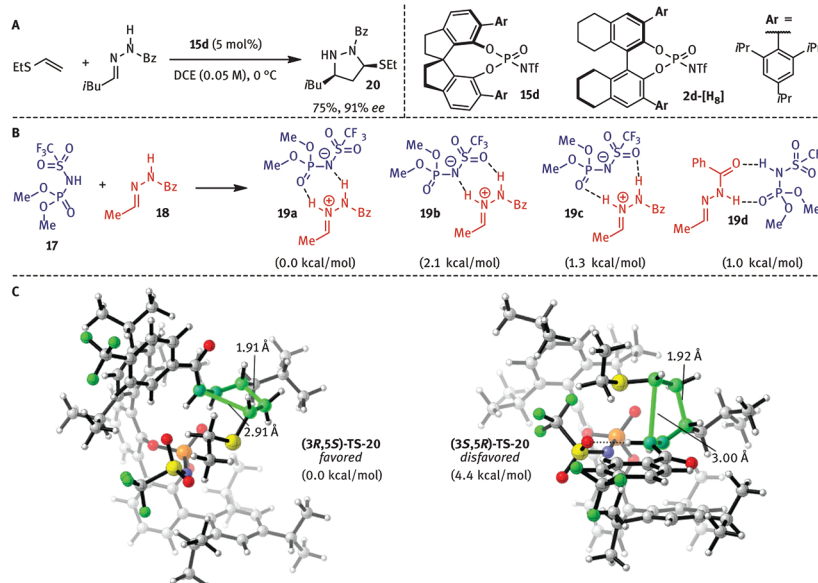


Figure 14: [3+2]-cycloaddition between hydrazones and alkenes catalyzed by NTPs. Adapted with permission from *J. Am. Chem. Soc.* **2014**, *136*, 13769.

Substitution of **17** with **2d-[H₈]** allowed computing the $\Delta\Delta G^\ddagger$ associated to the reaction enantioselectivity for the attack of ethyl vinylthioether to **18**. The coordination mode **19c** was conserved and a $\Delta\Delta G^\ddagger = 4.4$ kcal/mol in favor of product (3*R*,5*S*)-**20** was computed in agreement with the generally high selectivity observed in this reaction. The structure of the two diastereomeric TSs (3*R*,5*S*)-TS-20 and (3*S*,5*R*)-TS-20 are reported in Figure 14(c). Even though the origin of the computed $\Delta\Delta G^\ddagger$ is not clear at a first glance, removing the nucleophile from the structures and comparing the energy of the two remaining hydrazone/**2d-[H₈]** complexes results in an energy difference of 5.5 kcal/mol. This value is comparable to the computed $\Delta\Delta G^\ddagger$ and therefore the authors concluded that the selectivity in this reaction mostly originates from the interactions occurring between the catalyst's substituents and the hydrazone.

2.4.2 Nazarov reaction

The enantioselective Nazarov cyclization is another example of reaction catalyzed by NTPs. This transformation was also used by Rueping and coworkers as a benchmark reaction to gain insights into the Brønsted law for CBAs-catalyzed transformations (see Section 2.1, Figure 2). The stereochemical model for this catalytic system was first rationalized computationally by Krenske and coworkers [38]. As discussed in the previous paragraph, the computational treatment of the conformational flexibility of NTPs is a key point. Divinylketone and NTP **21** were used as model systems for a conformational analysis of a general catalyst/substrate complex **22** (Figure 15(a)). Interestingly, it was found that, differently from the [3+2] hydrazone cycloaddition reaction, the coordination of divinylketones occurs through either one of the tautomeric forms O=P-NH **22a** or TfN=P-OH **22b** of the NTP. However, while the Gibbs free energy difference between the two conformers at the ground state was negligible (0.5 kcal/mol in favor of **22b**), this energy difference was found to increase at the TS level (3.1 kcal/mol in favor of the TfN=P-OH form, Figure 15(a)). With evidence for the involvement of a tautomeric species like **22b** at the TS level, Kriske and coworkers studied the reaction of substrate **23** in the presence of NTP **24** (Figure 15(b)). The two diastereomeric TSs (**S**)-TS-**23** and (**R**)-TS-**23** for the conrotatory cyclization step, are reported in Figure 15(c). A $\Delta\Delta G^\ddagger = 1.4$ kcal/mol in favor of (**S**)-TS-**23** was calculated, which is in agreement with the experimental selectivity. Further interaction/distortion analysis of the two TSs allowed accessing more detailed information about the origin of the computed $\Delta\Delta G^\ddagger$. Distortion of the catalyst was found to be pivotal, being much stronger in the disfavored structure (**R**)-TS-**23**. Specifically, distortion of the N-triflyl phosphoramidate group alone was computed to account for a $\Delta\Delta E_{\text{distTf}}^\ddagger = 4.8$ kcal/mol. Interestingly, the discrepancy between the computed $\Delta\Delta E^\ddagger$ and $\Delta\Delta E_{\text{distTf}}^\ddagger$ suggests that interactions between the catalyst and the substrate are in favor of (**R**)-TS-**23**. This is in contrast with the case studies examined so far where the interaction energy is responsible for the enantiodiscrimination towards the favored product. Thus, this example shows how in CBA catalysis the selectivity is often dependent on many factors which go beyond the ability of these catalysts to engage the substrate in non-covalent interaction networks.

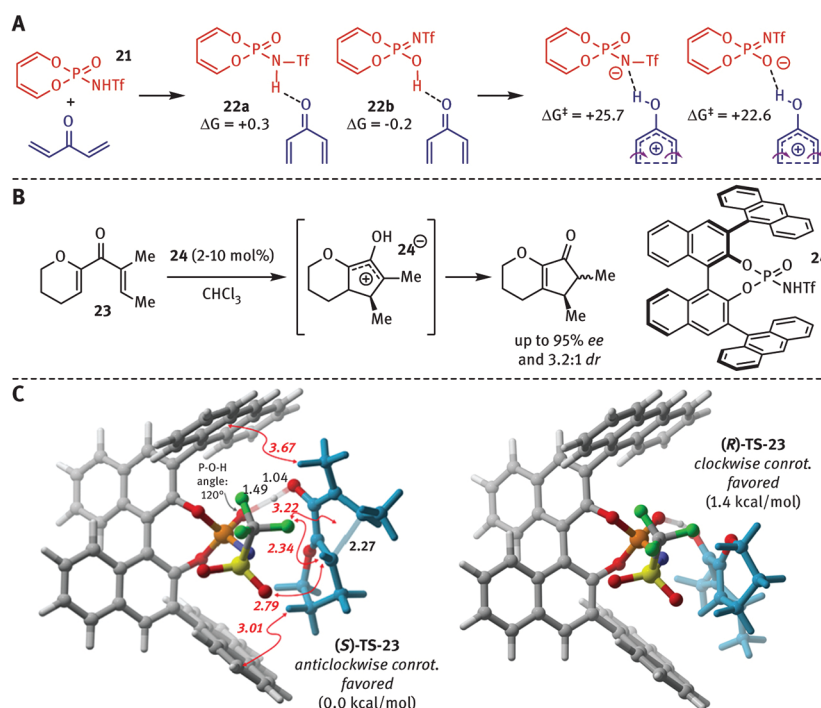


Figure 15: NTPs-catalyzed enantioselective Nazarov reaction. Adapted with permission from *ACS Catal.* 2017, 7, 3466.

2.4.3 Benzidine rearrangement

The enantioselective benzidine rearrangement of dinaphthylhydrazines catalyzed by CPAs was reported simultaneously by the groups of List and Kürti [39, 40]. They addressed the synthetic utility of this reaction that allows accessing enantioenriched BINAM derivatives from substrates **25** (Figure 16(a)). The two groups also undertook studies that provided interesting insights into the reaction mechanism from different perspectives. List and coworkers reasoned about the stoichiometry of the ionic pairing generated by the substrate and catalyst **1g**. Hydrazines **25** have two basic N atoms which could be protonated by the CPA. Thus, even though the

second protonation would be less favorable, two possible mechanistic pathways can be depicted in which only one or two phosphate molecules are involved in the sigmatropic rearrangement (Figure 16(b)). In order to gain insights about the hypothesized mechanisms the authors undertook a non-linear effect experiment, in which the product *ee* was measured with **1g** at different optical purities. The plot of the product *ee* against the catalyst *ee* resulted in a non-linear correlation, implying the actual presence of a reaction pathway involving more than one phosphate molecules at the stereodetermining step (Figure 16(b)). It is worth noticing, that the observed non-linear effect does not exclude the presence of a one-phosphate mechanism. In fact, the interplay of multiple mechanisms or the presence of dimeric pathways where the rearrangement occurs within H-bonded aggregates of more catalyst/substrates molecules is consistent with the experiment outcome.

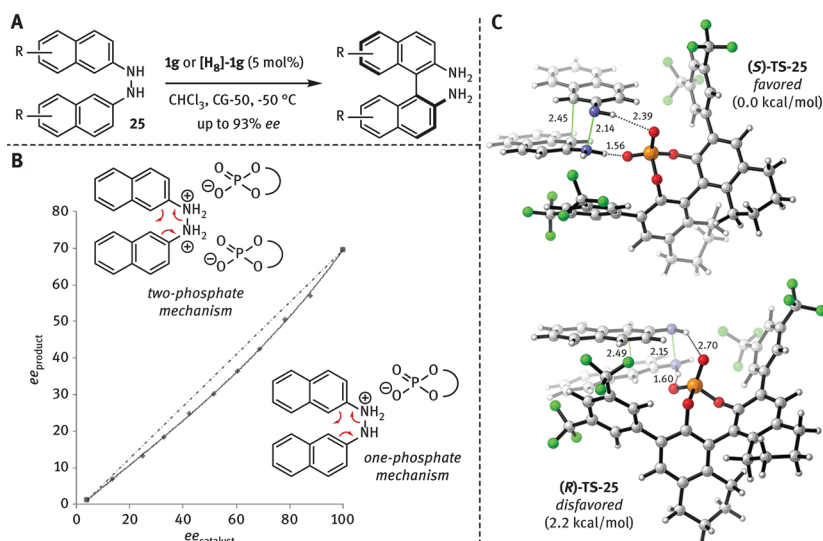


Figure 16: Enantioselective benzidine rearrangement of dinaphthylhydrazines catalyzed by CPAs. Adapted with permission from *Angew. Chem. Int. Ed.* **2013**, 52, 9293 and *J. Am. Chem. Soc.* **2013**, 135, 7414.

Kürti and coworkers performed a computational analysis of the one-phosphate mechanism. The computed TSs that involves the rearrangement of **25** in the presence of $[H_8]-1g$ ((S)-TS-25 and (R)-TS-25) are depicted in Figure 16(c). The $\Delta\Delta G^\ddagger$ associated to the reaction enantioselectivity is 2.2 kcal/mol. The energy difference was ascribed to the presence of CH- π interactions between the hydrazine aryl CH and the catalyst's electron-poor aryl substituents.

2.5 Stereoselective sulfoxidations

The enantioselective sulfoxidation reaction catalyzed by CBAs was first reported by List and coworkers in 2012 [41]. A wide set of CPAs was found to activate H_2O_2 toward thioanisoles to access sulfoxides albeit in low *ee* values (e. g. only 16% *ee* was obtained with catalyst **1H**). Higher selectivity was obtained by means of imidodiphosphoric acid **26** (Figure 17(a)), which provided oxidation of thioanisole **27** in 98% *ee*. In order to understand the mode of action of this new class of CBAs, computational studies were undertaken by the group of Sunoj [42]. Calculations showed that the reaction proceeds by coordination of H_2O_2 by the catalyst and consequent reaction of this complex with the substrate according with the mechanism in Figure 17(b). Computational prediction of the reaction enantioselectivity with (S)-**1H** resulted in structures (S)-TS1h-27 and (R)-TS1h-27, with an energy difference $\Delta\Delta G^\ddagger = 0.5$ kcal/mol in favor of (R)-TS1h-27, in agreement with the low *ee* obtained with this catalyst. On the other hand, the computed $\Delta\Delta G^\ddagger$ for the reaction catalyzed by **26** was as high as 3.9 kcal/mol, and consistent with the ideal selectivity obtained experimentally. Analysis of structures (S)-TS25-27 and (R)-TS25-27 compared to (S)-TS1h-27 and (R)-TS1h-27 highlighted the reasons for the higher efficiency of **26** with respect to **1H** (see Figure 17(c), grey = catalyst, red = O atoms, blue = substrate). While **1H** has an open pocket that results in conformational freedom at the TS level with consequent low selectivity, the chiral pocket of catalyst **26** is closed and resembles the active site of an enzyme.

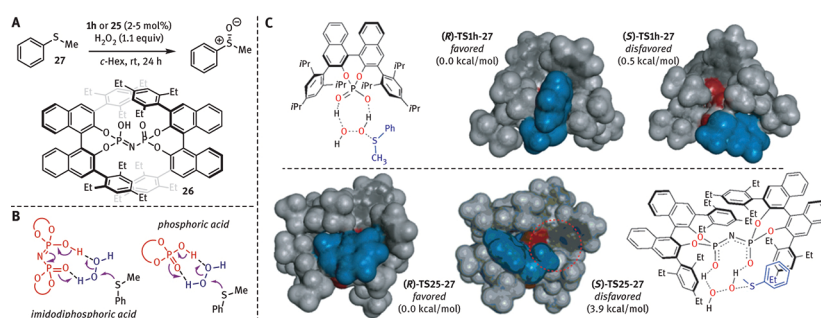


Figure 17: Enantioselective sulfoxidation reaction catalyzed by CBAs. Computational comparison between CPAs and imidodiphosphoric acids. Adapted with permission from *Angew. Chem. Int. Ed.* **2014**, *53*, 4432.

Further comparative analysis of (*S*)-**TS25-27** and (*R*)-**TS25-27** using the Van der Waals radii visualization mode, shows a better fitting of the substrate molecule into the catalyst's pocket in (*R*)-**TS25-27** (Figure 17(c), poor fitting for (*S*)-**TS25-27** highlighted by a red circle). This better fitting allows maximization of non-covalent interactions at the TS level, which results in the observed preference for the (*R*)-product.

3 Chiral counter-anion catalysis

3.1 Meso-Aziridinium and meso-episulfonium ring opening reactions

Counter-anion directed catalysis is based on the formation of a tight ion pair between a positively charged reaction intermediate and a chiral counter-anion from the catalyst [43]. The formation of such ion pair is dependent on several factors, reaction temperature and solvent properties being the most important. Indeed, for the ion pair to be formed, the energy associated with the electrostatic attraction between the two partners has to be larger than the thermal energy available to separate them. For this reason, chiral counter-anion directed reactions are performed in non-polar solvents (toluene, DCM, CHCl_3 , alkanes, etc.) and at low/moderate temperatures (typically not higher than r.t.). The first computational report assessing these concepts in the field of asymmetric catalysis is due to Duarte and Paton [44]. These authors studied the aziridinium and episulfonium ring opening reactions catalyzed by the phosphate anion of **1H** (Figure 18(a)). In these reactions the transient cationic reaction intermediates **28a-28b** are formed by abstraction of a chloride anion by Ag_2CO_3 from the starting material. Subsequent nucleophilic attack by an alcohol nucleophile leads to the formation of the desired aminoether or thioether in high enantioselectivity (91–94% *ee*). The study began with the evaluation by means of molecular dynamics (ΔG_{MD}) and DFT (ΔG_{DFT}) of the ion pair Gibbs free energy of association in various solvents (toluene, DCM, MeCN and H_2O). Not surprisingly, the calculated values were found to correlate with the corresponding dielectric constants and are listed in Figure 18(b). The coordination mode of **28a** and **28b** by **1H** is reminiscent of the complexation of the epoxides in (*S,S*)-**TS1h-14** and (*R,R*)-**TS1h-14** (Figure 10). Also in this case, the three membered ring H atoms were found to be involved in a direct electrostatic interaction with the phosphate anion, leading to a rigid and tight ionic complex (Figure 18(b)).

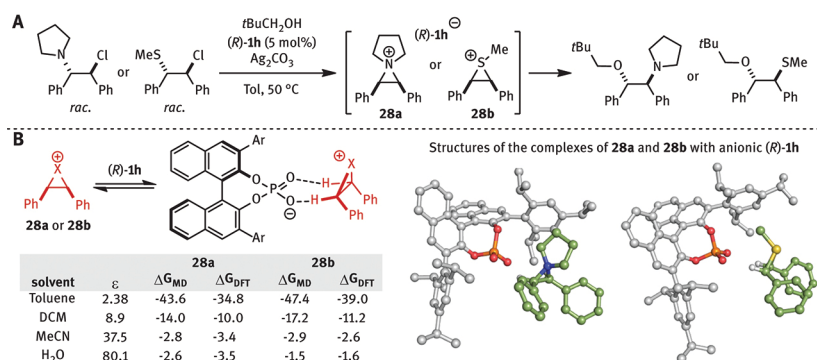


Figure 18: *meso*-aziridinium and *meso*-episulfonium ring opening reactions by counter-anion directed catalysis. Adapted with permission from *J. Am. Chem. Soc.* **2017**, *139*, 8886.

Due to the *meso* relative configuration of intermediates **28**, attack of the nucleophile to one of the two C atoms leads to opposite enantiomers of the desired product. Due to the chiral environment provided by catalyst (*R*)-**1H**, the attack occurs at the (*R*)-carbon leading to the preferential formation of the (*S,S*)-product. The structure

of the diastereomeric TSs for the attack to **28a** ((*S,S*)-TS-28a and (*R,R*)-TS-28a) and **28b** ((*S,S*)-TS-28b and (*R,R*)-TS-28b) are reported in Figure 19. The $\Delta\Delta G^\ddagger$ associated to the reaction enantioselectivity is 2.1 kcal/mol for **28a** and 5.4 kcal/mol for **28b**, in agreement with the high *ee* obtained experimentally. Interaction/distortion analysis revealed that the selectivity is almost exclusively due to a stronger substrate distortion in (*R,R*)-TS-28b.

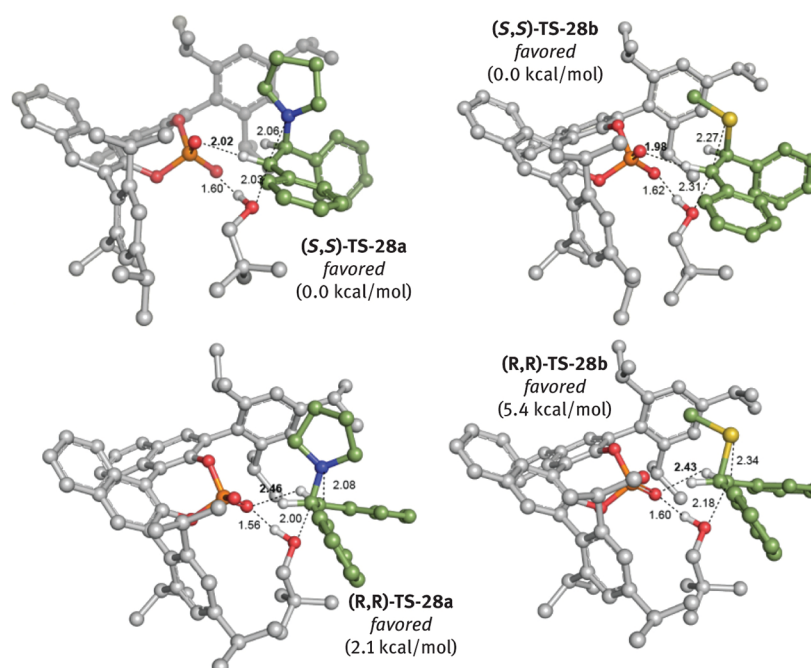


Figure 19: Computed TSs for the TRIP-counterion catalyzed ring opening reaction of meso-aziridinium and meso-episulfonium. Reproduced with permission from *J. Am. Chem. Soc.* **2017**, 139, 8886.

3.2 Stereoselective fluorination of allylic alcohols

In 2014, Toste and coworkers developed an in situ directing group strategy to access the enantioselective fluorination of allylic alcohols in high enantioselectivity [45]. In this reaction, **Selectfluor** was used as the fluorinating agent under chiral anion phase transfer regime with a chiral phosphate as catalyst. An arylboronic acid **BA** was added as additive to the reaction, which in the presence of the substrate **29** was shown to form a mixed boronic ester **30**. Such intermediate is the actual substrate that undergoes fluorination to give product **31** after a hydrolytic workup. The pattern substitution of **BA** strongly affected the reaction selectivity, which was shown to reverse upon substitution of the *meta*-positions of the aryl group (Figure 20(a)). In order to gain mechanistic understanding of the manifold at the basis of this reaction, the groups of Toste and Sigman undertook a mechanistic study [46]. Non-linear effect experiments showed that chiral phosphates with *ortho*-substituents at the 3,3'-aryl substituents (**1H**, **1I**, **1m** and **1H**, Figure 20(a)) behaved differently from unsubstituted ones. Specifically, the former ones did not give non-linear effects, differently from other catalysts. Thus, only catalysts **1H**, **1I**, **1m** and **1H** were selected for further studies, as these showed to work with the same mechanism. A stereochemical model for this transformation was developed [18] by means of DFT calculations and Multidimensional Correlation Analysis (MCA) [47, 48]. In this approach, experimental *ee* values are correlated through multidimensional regression analysis to a set of computationally acquired parameters. The resulting polynomial equation contains those parameters that describe the features of the catalyst/substrate that affect the reaction stereochemical outcome. Therefore, mechanistic information can be obtained by the analysis of such descriptors.

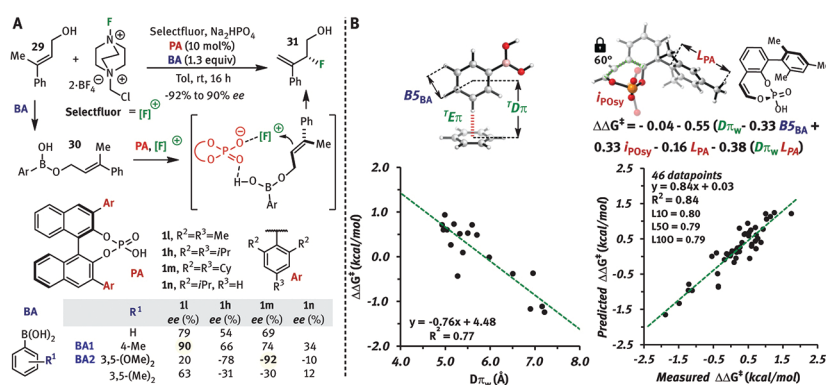


Figure 20: Correlation analysis of the enantioselective fluorination of allylic alcohols catalyzed by CPAs anions. Adapted with permission from *J. Am. Chem. Soc.* **2017**, 139, 6803.

Application of MCA to a dataset of 46 catalyst/BA combinations resulted in the model depicted in Figure 20(c). The parameters include $^T D\pi_w$, accounting for geometric requirements derived from the apparent presence of a π interaction (Figure 20(b)); $B5_{BA}$ and L_{PA} , Sterimol values describing steric effects from BA and the catalyst, respectively; and, i_{POsy} , the phosphate symmetric stretching intensity, which represents the ability of each phosphate to engage in H-bonding/electrostatic interactions. The coefficients of the model equation suggest the T-shaped π -stacking interaction engaged by the *meta*-position of BA to be important. Furthermore, simple correlation of $^T D\pi_w$ against the experimental enantioselectivity (Measured $\Delta\Delta G^\ddagger$ expressed in kcal/mol) showed a quantitative trend with $R^2 = 0.77$ (Figure 20(b)). Thus, based on this parameters analysis, a TS involving i) a π -stacking between the BA *meta*-substituent and the catalyst BINOL scaffold, and ii) H-bond/electrostatic interaction between the catalyst phosphate moiety, Selectfluor and BA was hypothesized.

In order to access visualization of the hypothesized TSs, DFT computations were undertaken combining catalyst 1H and BA1 or BA2. Remarkably, this DFT study revealed that TSs presenting a T-shaped interaction between the aryl ring of BA1 and the BINOL scaffold of 1H are the lowest in energy. The favored TSs leading to the R and S products are depicted in Figure 21(a), with (R)-TSBA1-30 leading to the major observed product (computed $\Delta\Delta G^\ddagger = 1.0$ kcal/mol; experimental $\Delta\Delta G^\ddagger = 0.9$ kcal/mol). Location of low-lying TSs was also performed for the 1H/BA2 system. The analysis showed that (R)-TSBA2-30 and (S)-TSBA2-30 (Figure 4(b)) are the lowest in energy, and the formation of the S enantiomer as the major product is consistent with the observed results (computed $\Delta\Delta G^\ddagger = 2.6$ kcal/mol; experimental $\Delta\Delta G^\ddagger = 1.2$ kcal/mol). Supporting the hypothesis resulting from the parameters found in the MCA analysis, T-shaped π -interactions between the *meta* substituent of BA2 and the BINOL moiety of 1H are present in both systems (Figure 21(b)). Moreover, H-bonding (a), π stacking (b), and electrostatics (c) interactions were found in the computed TSs (Figure 21), which can be connected to the parameters i_{POsy} (a and c), and $^T D\pi_w$ and $B5_{BA}$ (b) of the MCA.

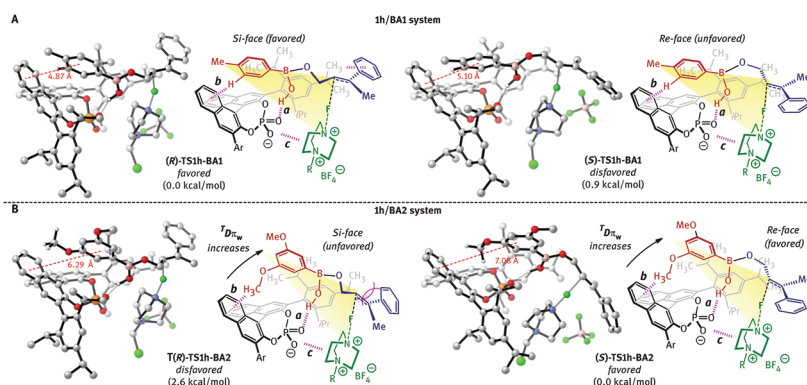


Figure 21: Computational analysis of the enantioselective fluorination of allylic alcohols catalyzed by TRIP. Reproduced with permission from *J. Am. Chem. Soc.* **2017**, 139, 6803.

3.3 Enantioselective Pummerer reaction

In the 2017, Sigman and Toste developed and studied an enantioselective Pummerer reaction based on a chiral anion phase transfer process [49]. In this reaction, a benzylic thioether 32 is oxidized *in situ* by an oxammonium salt 33 in the presence of chiral phosphate 1o. The resulting thionium cation forms a tight ion pair

34 with the phosphate **10**, and undergoes a stereoselective cyclization to give the desired product **35** (Figure 22(a)). The reaction proceeded with moderate to good enantioselectivity over a wide range of substrates and catalysts, which prompted the authors to study the reaction via a combined MCA and DFT approach. MCA was performed separately on a *ee* values dataset obtained with substrate **32** and 12 different catalysts (Figure 22(b)). Three Sterimol parameters appeared in the equation: **B5**, maximum width of the entire catalyst's aryl substituent; **B1₂** and **B1₄**, minimum width of the substituents in the *ortho*-positions and of the substituent in the *para*-position of the aryl group, respectively. These parameters describe the requirement for a proper steric environment into the catalyst's chiral pocket. Additional insights into the stereochemical recognition were obtained by MCA of the ion pair cationic counterpart. Descriptors for a set of nine substrates with different aryl groups at the sulfonamide moiety were calculated from the TS of the corresponding thionium cation in the uncatalyzed cyclization. The analysis resulted in the statistical model in Figure 22(c), which contains two parameters condensed into one term. These parameters accounts for either the steric hindrance or the shape of the aryl substituent (**B5_{Ar}**), and the average charge of the thionium alkyl chain (**NBO_{AlkH}**). The presence of this latter descriptor in the model suggested the presence of non-covalent interactions at the TS level involving the alkyl chain next to the thionium moiety.

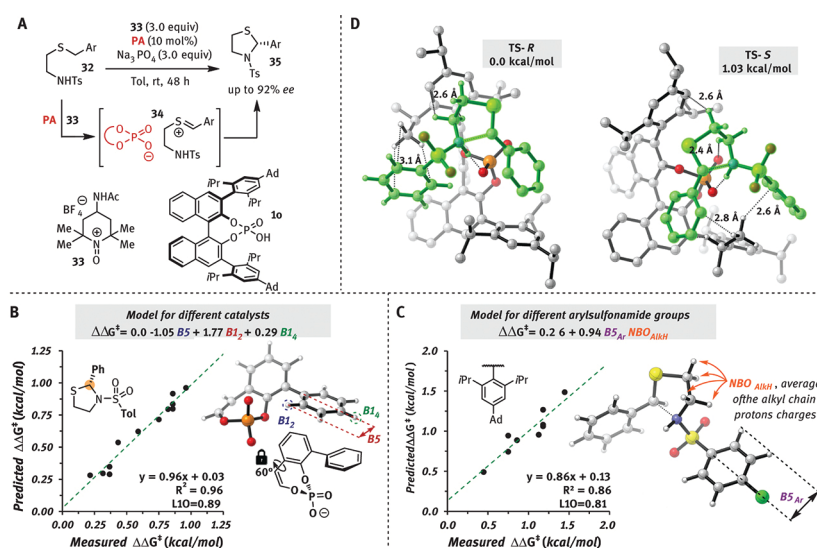


Figure 22: Enantioselective Pummerer reaction via Chiral Anion Phase Transfer Catalysis, and its computational/MCA analysis. Adapted with permission from *Angew. Chem. Int. Ed.* **2018**, *57*, 589.

Further information about the interaction mode between the catalyst and the substrate was gained by DFT computation of the reaction TSs involving **32** and **1H**. The low-lying TSs leading to the *R*- and *S*-configured products (**(R)-TS-32** and **(S)-TS-32**, respectively) are depicted in Figure 22(d) (substrate highlighted in green). **(R)-TS-32** is favored and consistent with the experimentally observed product configuration, and the relative energy of **(S)-TS-32** (1.03 kcal/mol) matched with the selectivity measured experimentally (56% *ee*, 0.75 kcal/mol). The two TSs showed several non-covalent interactions between the phosphate and the substrate. However, **(R)-TS-32** displayed a better accommodation of the benzenesulfonamide group through CH- π interactions, which involved the *iPr* substituents and the binaphthyl backbone of the catalyst. This representation provides an interpretation for the statistical model in Figure 22(b), where strict requirements about the catalyst's substituents were highlighted. Additionally, a stronger CH- π interaction between the aryl substituent or **1H** (*iPr*₃Ph) and the electron-deficient alkyl chain of the cationic intermediate was present in **(R)-TS-32** (three CH- π contacts, while **(S)-TS-32** presented only one CH- π contact). The presence of these interactions in the computed TSs is fully consistent with the model equation obtained by MCA in Figure 22(c).

4 General considerations

In the last twenty years, CBA and chiral counteranion catalysis have emerged as a fundamental area of organocatalysis. The development of chiral acidic catalysts has allowed extending many known Brønsted catalyzed reactions to the stereoselective domain. Moreover, the controlled conditions under which these catalysts can be used, allowed accessing reactivity of increasing complexity with extraordinary selectivity levels. For instance, the development of bisimidophosphoric acids by List allowed accessing reactivity of new substrates within the tight catalyst pocket, which is reminiscent of enzymatic catalysis [50]. Exploitation of the solubility

of bulky CPAs allowed Toste and coworkers to develop the chiral counteranion phase transfer catalysis [51], where the low solubility of the starting material allows high control of background reactions of highly reactive reagents. However, compared to the fast growth of these fields in an applicative fashion, only little has been done in order to understand the mode of action of these new catalysts. Part of the work reported in this direction was reviewed in this chapter, with examples from both CBA and counteranion directed catalysis. The contributions summarized here allow outlining several key points about the use of chiral phosphates in catalysis.

Studies by Leito and Rueping highlighted the importance of the catalyst's acidity for accessing desirable levels of reactivity. Indeed, for the Nazarov cyclization, it has been shown that the reaction rate follows the Brønsted law. However, acidity alone is not sufficient for achieving a good control of the reaction selectivity. In fact, Gschwind and coworkers showed that the success of CPAs with respect of other possible acidic functional groups is due to the properties of the H-bond that phosphates can form. In particular, it was shown that phosphates can engage H-bonds with iminium ions that are stronger with respect to those formed by other acidic compounds. The same team showed that BINOL-based phosphates are able to coordinate iminium ions by non-covalent interactions thanks to their extended π -systems. Computational analysis of a variety of CBA catalyzed reactions by Goodman, Houk, Wheeler, Sunoj, and others allowed assessing the importance of these features for optimal molecular recognition at the TS level, rationalizing the high levels of selectivity experimentally accessed by CPAs. On the other hand, it was shown that the activation mode and the coordination of the substrate by these catalysts is often difficult to predict. Indeed, differently from covalent catalysis, the interactions interplaying at the TS level are strongly dependent on the features of the electrophile, including steric, electronic and substitution patterns. For this reason, the continuous development of new methodologies and physical organic techniques (for instance as pioneered by Gschwind and Sigman) aiming the study and understanding of these catalytic systems is a topic of major importance in the field of organocatalysis.

References

- [1] Brønsted JN, Pedersen KJ. Die katalytische Zersetzung des Nitramids und ihre physikalisch-chemische Bedeutung. *Zeitschrift für Phys Chemie Stöchiometrie und Verwandtschaftslehre*. 1924;108:185–235.
- [2] Kütt A, Leito I, Kaljurand I, Sooväli L, Vlasov VM, Yagupolskii LM, et al. A comprehensive self-consistent spectrophotometric acidity scale of neutral Brønsted acids in acetonitrile. *J Org Chem*. 2006;71:2829–38.
- [3] Kütt A, Rodima T, Saame J, Raamat E, Mäemets V, Kaljurand I, et al. Equilibrium acidities of superacids. *J Org Chem*. 2011;76:391–5.
- [4] Christ P, Lindsay AG, Vormittag SS, Neudörfl JM, Berkessel A, O'Donoghue AC. K_a values of chiral Brønsted acid catalysts: phosphoric acids/ amides, sulfonyl/sulfonyl imides, and perfluorinated TADDOLs (TEFDDOLs). *Chem Eur J*. 2011;17:8524–8.
- [5] Kaupmees K, Tolstoluzhsky N, Raja S, Rueping M, Leito I. On the acidity and reactivity of highly effective chiral Brønsted acid catalysts: establishment of an acidity scale. *Angew Chem Int Ed*. 2013;52:11569–72.
- [6] Yang C, Xue XS, Jin JL, Li X, Cheng JP. Theoretical study on the acidities of chiral phosphoric acids in dimethyl sulfoxide: hints for organocatalysis. *J Org Chem*. 2013;78:7076–85.
- [7] Yang C, Xue XS, Li X, Cheng JP. Computational study on the acidic constants of chiral Brønsted acids in dimethyl sulfoxide. *J Org Chem*. 2014;79:4340–51.
- [8] Uruguchi D, Terada M. Chiral Brønsted acid-catalyzed direct Mannich reactions via electrophilic activation. *J Am Chem Soc*. 2004;126:5356–7.
- [9] Akiyama T, Itoh J, Yokota K, Fuchibe K. Enantioselective Mannich-type reaction catalyzed by a chiral Brønsted acid. *Angew Chem Int Ed*. 2004;43:1566–8.
- [10] Fleischmann M, Drettwan D, Sugiono E, Rueping M, Gschwind RM. Brønsted acid catalysis: hydrogen bonding versus ion pairing in imine activation. *Angew Chem Int Ed*. 2011;50:6364–9.
- [11] Kim H, Sugiono E, Nagata Y, Wagner M, Bonn M, Rueping M, et al. Role of ion-pairs in Brønsted acid catalysis. *ACS Catal*. 2015;5:6630–3.
- [12] Sorgenfrei N, Hioe J, Greindl J, Rothermel K, Morana F, Lokesh N, et al. NMR spectroscopic characterization of charge assisted strong hydrogen bonds in Brønsted acid catalysis. *J Am Chem Soc*. 2016;138:16345–54.
- [13] Sharif S, Denisov GS, Toney MD, Limbach H. Coupling of functional hydrogen bonds in pyridoxal-5'-phosphate—enzyme model systems observed by solid-state NMR spectroscopy. *J Am Chem Soc*. 2007;129:6313.
- [14] Limbach HH, Pietrzak M, Sharif S, Tolstoy PM, Shenderovich IG, Smirnov SN, et al. NMR parameters and geometries of OHN and ODN hydrogen bonds of pyridine—acid complexes. *Chem Eur J*. 2004;10:5195.
- [15] Benedict H, Shenderovich IG, Malkina OL, Malkin VG, Denisov GS, Golubev NS, et al. Nuclear scalar spin—spin couplings and geometries of hydrogen bonds. *J Am Chem Soc*. 2000;122:1979.
- [16] Limbach HH, Pietrzak M, Benedict H, Tolstoy PM, Golubev NS, Denisov GS. Empirical corrections for quantum effects in geometric hydrogen bond correlations. *J Mol Struct*. 2004;706:115.
- [17] Greindl J, Hioe J, Sorgenfrei N, Morana F, Gschwind RM. Brønsted acid catalysis—structural preferences and mobility in imine/phosphoric acid complexes. *J Am Chem Soc*. 2016;138:15965–71.
- [18] Orlandi M, Coelho JA, Hilton MJ, Toste FD, Sigman MS. Parametrization of non-covalent interactions for transition state interrogation applied to asymmetric catalysis. *J Am Chem Soc*. 2017;139:6803–6.

- [19] Rueping M, Sugiono E, Azap C, Theissmann T, Bolte M. Enantioselective Brønsted acid catalyzed transfer hydrogenation: organocatalytic reduction of imines. *Org Lett*. 2005;7:3781–3.
- [20] Hoffmann S, Seayad AM, List B. A powerful Brønsted acid catalyst for the organocatalytic asymmetric transfer hydrogenation of imines. *Angew Chem Int Ed*. 2005;44:7424–7.
- [21] Simón L, Goodman JM. Theoretical study of the mechanism of Hantzsch ester hydrogenation of imines catalyzed by chiral BINOL-phosphoric acids. *J Am Chem Soc*. 2008;130:8741–7.
- [22] Marcelli T, Hammar P, Himo F. Hantzsch esters employed for asymmetric imine reduction. *Adv Synth Catal*. 2009;351:525–9.
- [23] Marcelli T, Hammar P, Himo F. Phosphoric acid catalyzed enantioselective transfer hydrogenation of imines: a density functional theory study of reaction mechanism and the origins of enantioselectivity. *Chem Eur J*. 2008;14:8562–71.
- [24] Reid JP, Goodman JM. Goldilocks catalysts: computational insights into the role of the 3,3' substituents on the selectivity of BINOL-derived phosphoric acid catalysts. *J Am Chem Soc*. 2016;138:7910–17.
- [25] Simón L, Goodman JM. Mechanism of BINOL–phosphoric acid-catalyzed strecker reaction of benzyl imines. *J Am Chem Soc*. 2009;131:4070–7.
- [26] Monaco MR, Poladura B, Diaz de Los Bernardos M, Leutzsch M, Goddard R, List B. Activation of carboxylic acids in asymmetric organocatalysis. *Angew Chem Int Ed*. 2014;53:7063–7.
- [27] Monaco MR, Prévost S, List B. Organocatalytic asymmetric hydrolysis of epoxides. *Angew Chem Int Ed*. 2014;53:8142–5.
- [28] Monaco MR, Prévost S, List B. Catalytic asymmetric synthesis of thiols. *J Am Chem Soc*. 2014;136:16982–5.
- [29] Monaco MR, Fazzi D, Tsuji N, Leutzsch M, Liao S, Thiel W, et al. The activation of carboxylic acids via self-assembly asymmetric organocatalysis: a combined experimental and computational investigation. *J Am Chem Soc*. 2016;138:14740–9.
- [30] Liao S, Leutzsch M, Monaco MR, List B. Catalytic enantioselective conversion of epoxides to thiranes. *J Am Chem Soc*. 2016;138:5230–3.
- [31] Seguin TJ, Wheeler SE. Competing noncovalent interactions control the stereoselectivity of chiral phosphoric acid catalyzed ring openings of 3-substituted oxetanes. *ACS Catal*. 2016;6:7222–8.
- [32] Yang W, Sun J. Organocatalytic enantioselective synthesis of 1,4-dioxanes and other oxa-heterocycles by oxetane desymmetrization. *Angew Chem Int Ed*. 2016;55:1868–1871.
- [33] Wang Z, Chen Z, Sun J. Catalytic asymmetric nucleophilic openings of 3-substituted oxetanes. *Org Biomol Chem*. 2014;12:6028–6032.
- [34] Yang W, Wang Z, Sun J. Enantioselective oxetane ring opening with chloride: unusual use of wet molecular sieves for the controlled release of HCl. *Angew Chem Int Ed*. 2016;55:6954–6958.
- [35] Maji R, Champagne PA, Houk KN, Wheeler SE. Activation mode and origin of selectivity in chiral phosphoric acid-catalyzed oxacycle formation by intramolecular oxetane desymmetrizations. *ACS Catal*. 2017;7:7332–9.
- [36] Champagne PA, Houk KN. Origins of selectivity and general model for chiral phosphoric acid-catalyzed oxetane desymmetrizations. *J Am Chem Soc*. 2016;138:12356–9.
- [37] Hong X, Küçük HB, Maji MS, Yang YF, Rueping M, Houk KN. Mechanism and selectivity of N-triflylphosphoramidate catalyzed (3+2) cycloaddition between hydrazones and alkenes. *J Am Chem Soc*. 2014;136:13769–80.
- [38] Lovie-Toon JP, Tram CM, Flynn BL, Krenske EH. Mechanisms of carbonyl activation by BINOL N-triflylphosphoramides: enantioselective Nazarov cyclizations. *ACS Catal*. 2017;7:3466–76.
- [39] Li GQ, Gao H, Keene C, Devonas M, Ess DH, Kürti L. Organocatalytic Aryl–Aryl bond formation: an atroposelective [3,3]-rearrangement approach to BINAM derivatives. *J Am Chem Soc*. 2013;135:7414–17.
- [40] De CK, Pescioli F, List B. Catalytic asymmetric benzidine rearrangement. *Angew Chem Int Ed*. 2013;52:9293–5.
- [41] Liao S, Čorić I, Wang Q, List B. Activation of H₂O₂ by chiral confined Brønsted acids: a highly enantioselective catalytic sulfoxidation. *J Am Chem Soc*. 2012;134:10765–8.
- [42] Jindal G, Sunoj RB. Axially chiral imidodiphosphoric acid catalyst for asymmetric sulfoxidation reaction: insights on asymmetric induction. *Angew Chem Int Ed*. 2014;53:4432–6.
- [43] Mahlau M, List B. Asymmetric counteranion-directed catalysis: concept, definition, and applications. *Angew Chem Int Ed*. 2013;52:518–33.
- [44] Duarte F, Paton RS. Molecular recognition in asymmetric counteranion catalysis: understanding chiral phosphate-mediated desymmetrization. *J Am Chem Soc*. 2017;139:8886–96.
- [45] Zi W, Wang YM, Toste FD. An *in Situ* directing group strategy for chiral anion phase-transfer fluorination of allylic alcohols. *J Am Chem Soc*. 2014;136:12864–7.
- [46] Neel AJ, Milo A, Sigman MS, Toste FD. Enantiodivergent fluorination of allylic alcohols: data set design reveals structural interplay between achiral directing group and chiral anion. *J Am Chem Soc*. 2016;138:3863–75.
- [47] Sigman MS, Harper KC, Bess EN, Milo A. The development of multidimensional analysis tools for asymmetric catalysis and beyond. *Acc Chem Res*. 2016;49:1292–301.
- [48] Santiago CB, Guo J-Y, Sigman MS. Predictive and mechanistic multivariate linear regression models for reaction development. *Chem Sci*. 2018;9:2398–412.
- [49] Biswas S, Kubota K, Orlandi M, Turberg M, Miles DH, Sigman MS, et al. Enantioselective synthesis of N,S-acetals by an oxidative pummerer-type transformation using phase-transfer catalysis. *Angew Chem Int Ed*. 2018;57:589–93.
- [50] Čorić I, List B. Asymmetric spiroacetalization catalysed by confined Brønsted acids. *Nature*. 2012;483:315.
- [51] Rauniyar V, Lackner AD, Hamilton GL, Toste FD. Asymmetric electrophilic fluorination using an anionic chiral phase-transfer catalyst. *Science*. 2011;334:1681–4.